IEEE Access
Multidisciplinary ⋮ Rapid Review ⋮ Open Access Journal

Received 27 February 2026, accepted 31 March 2026, date of publication 10 April 2026, date of current version 27 April 2026.

Digital Object Identifier 10.1109/ACCESS.2026.3682800

RESEARCH ARTICLE

High-Gain Wide-Angle Scanning Array Using Slot-Based Patch Antenna for Ku-Band

AMIT MEHTA[1], (Senior Member, IEEE), RAWAD W. ASFOUR[2], (Member, IEEE), HISAMATSU NAKANO[3], (Life Fellow, IEEE), AND DARIUSH MIRHSEKAR-SYAHKAL[2], (Life Fellow, IEEE)

[1]Electronic and Electrical Engineering Department, Swansea University, Swansea, U.K.
[2]School of Computer Science and Electronic Engineering (CSEE), University of Essex, Colchester, U.K.
[3]Department of Electrical and Electronics, Science and Engineering, Hosei University, Tokyo, Japan

Corresponding author: Rawad W. Asfour (r.asfour@essex.ac.uk)

This work was supported in part by the Engineering and Physical Sciences Research Council (EPSRC) under Grant EP/X041395/1, and in part by ESA.

ABSTRACT High-gain wide-angle scanning antennas are vital for emerging Ku-band satellite communication systems supporting mobile, IoT, and UAV platforms. However, achieving compactness, circular polarization, and stable gain over a wide scanning range remain a key design challenge. This paper presents a Slot-Based Microstrip Patch Antenna (SBMPA) array optimized for high-gain, reconfigurable circularly polarized (CP) operation in the Ku-band (12.85–13.05 GHz). Each SBMPA element integrates a slotted circular patch nested inside a concentric annular ring operating in the TM_{11} (axial) and TM_{21} (conical) modes, respectively. With a quadrature-feed network, the antenna generates a tilted CP beam ($\theta = 35°$) with a gain of 6.8 dBic and has the potential to switch between right-hand circular polarization (RHCP), left-hand circular polarization (LHCP), and linear polarization (LP) (which is not considered in this paper). A four-element linear SBMPA array, controlled through a phase-shift network, is shown to achieve beam steering up to $-47°$ with -3 dB coverage extending to $-60°$, while maintaining a stable gain ranging from 9.1 to 11.2 dBic across the entire scanning range and low sidelobe levels (–9 dB). The proposed array can offer a compact, polarization-agile solution with robust performance, making it suitable for low-profile satellite terminals and near-horizon communication in next-generation Ku-band applications.

INDEX TERMS Microstrip patch antenna, array antenna, beam steering, circular polarization, wide-angle scanning.

I. INTRODUCTION

Wide-angle scanning phased array antennas [1], [2] are highly desirable in various civil and defense applications, including satellite communication, terrestrial microwave communication [3], and radar systems [4], particularly for vehicular connectivity [5]. However, existing antenna solutions for satellite terminal connectivity [6] are generally unable to scan the beam efficiently at low elevation angles ($\theta > 40°$, where θ is the elevation angle measured from the zenith). The scanning range of a typical square or rectangular half-wavelength ($\lambda g/2$) patch antenna array is limited to approximately 40° from the zenith. Beyond this limit, the antenna beam exhibits significant grating lobes, accompanied by a gain reduction exceeding 3 dB [7], [8], [9]. Such systems often depend on bulky mechanical gimbals to extend the scanning range beyond $\theta > 40°$, which increases system complexity and susceptibility to mechanical failure. To achieve near-horizon wide-angle scanning, several approaches have been proposed [10], [11], [12]. Nevertheless, most radiating elements in these methods produce primarily axial beams and consequently exhibit lower gain at lower elevation angles. More recently, pattern-reconfigurable antenna arrays have gained considerable attention due to their ability to achieve wide scanning ranges with high-gain beam steering at low elevations [13], [14], [15]. For instance, the array in [14]

The associate editor coordinating the review of this manuscript and approving it for publication was Sandra Costanzo.

employs switched-pattern square loop antennas to cover a wide scanning range of $-60° < \theta < +60°$ with low grating lobes. The arrays in [13] and [14] are linearly polarized, with unit elements relying on discrete steering states. The array in [15] is circularly polarized (CP) with a switched beam, but it suffers from a gain variation of approximately 4 dB when steered in the azimuth plane and lacks polarization reconfigurability. Recent developments in Ku-band antenna design have focused on compact, wideband, and polarization-agile configurations to address these challenges. Several dual-polarized Ku-band antennas have demonstrated improved port isolation and enhanced impedance bandwidth, contributing to more reliable satellite communication links [16]. Comprehensive reviews of Ku-, K-, and Ka-band antenna technologies have also highlighted advancements in circularly polarized, frequency-reconfigurable, and miniaturized designs, emphasizing their importance in CubeSat and small satellite platforms [17]. Moreover, low-profile dual-circularly polarized antenna arrays have been explored to achieve high isolation and stable gain performance while maintaining a compact structure, making them suitable for integration into modern satellite and mobile communication terminals [18]. To overcome the combined limitations of low gain steering off boresight and limited polarization reconfigurability, novel antenna configurations have been investigated, including reconfigurable multimode hybrid patch antennas [19], [20], [21] and Slot-Based Microstrip Patch Antennas (SBMPAs) supporting circular polarization [18]. The works in [19], [20], [21] focus primarily on single-element designs intended for null steering. The present work builds upon [18] and extends the concept by introducing a circularly polarized array employing multimode hybrid SBMPA elements for beam steering in the Ku-band. Unlike conventional microstrip patch arrays that rely solely on array size to enhance gain, the proposed design achieves high gain through a combination of element-level radiation shaping and array-factor enhancement. At the element level, the SBMPA excites both the TM_{11} axial mode and the TM_{21} conical mode, whose constructive superposition produces a directive tilted beam with enhanced off-broadside radiation. At the array level, coherent combination of these tilted element patterns through controlled phase excitation further increases the overall directivity, enabling stable high-gain performance over wide scanning angles without the use of reflectors or superstrates. Sec. II outlines the design and optimization of the SBMPA element required for the target frequency band. Sec. III investigates a 1×4 linear SBMPA array to demonstrate high-gain, wide-angle scanning performance. A fabricated SBMPA array prototype and its feed system are also presented for experimental validation of the simulated results.

II. DESIGN OF THE ANTENNA ELEMENT

The SBMPA, Figure 1, comprises two sections that operates in two independent modes on a common radiating aperture [21]. It consists of a slotted circular patch nested within an annular ring (patch) on the same substrate as shown in Figure 1. The circular patch operates in TM_{11} and the annular ring operates in TM_{21}. In this work the SBMPA conductor is patterned on Rogers RO4350B substrate ($\varepsilon_r = 3.48$ and $\tan\delta = 0.003$ and $h = 1.02$ mm) of square shape with side lengths $W = 16$ mm ($0.68\ \lambda$ at 12.85 GHz). To design the SBMPA in Ku-band, the same topology and design techniques as [21] are used. Given the complexity of the SBMPA design, analytical methods alone cannot generate an optimal design. Therefore, a systematic iterative optimization procedure was employed, where key parameters (slot dimensions, patch radius, and feed locations) were varied stepwise while monitoring S-parameters, axial ratio, and radiation patterns, until the desired performance was achieved. From this process, it was found that the inner circular patch requires a radius of $r_1 = 2.516$ mm. On this patch there are eight slots with length and width of $SL = 1.628$ mm and $S_W = 0.5624$ mm respectively, distributed at an angular separation of 45°. The outer radius of the annular patch is $r_2 = 5.77$ mm. The isolation gap between the two patches is $g = 0.296$ mm. The optimized geometrical parameters are summarized in Table 1.

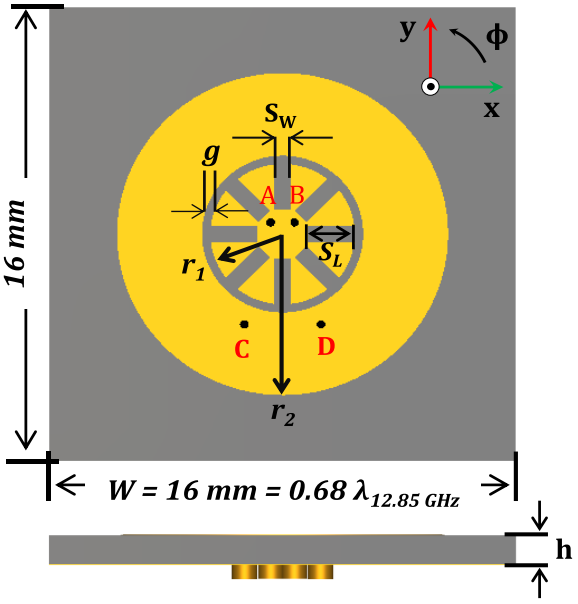

FIGURE 1. Geometry of the proposed SBMPA: (a) top view and (b) side view.

The performance of the designed SBMPA is simulated using CST Microwave Studio [22]. Figure 2 shows the simulated reflection coefficients ($|S_{xx}|$) and mutual coupling ($|S_{xy}|$) for the TM_{11} and TM_{21} modes of the SBMPA. When ports A and B are excited and ports C and D terminated into 50 Ω, the circular patch can provide an impedance bandwidth of 1.5% (12.85 – 13.05 GHz) for the $|S11| < -10$ dB criterion. The outer annular ring can offer an impedance bandwidth of 2.3% (12.8 – 13.1 GHz) when the excitation is on ports C and D with the other two ports terminated into 50 Ω. The mutual coupling levels amongst

TABLE 1. Optimized geometrical parameters of the proposed SBMPA element.

Symbol	Quantity	Value (mm)
h	Substrate thickness	1.02
ε_r	Substrate dielectric constant	3.48
W	Antenna side length	16
r_1	Inner circular patch radius	2.516
r_2	Outer ring radius	5.77
S_L	Slot length	1.628
S_W	Slot width	0.5624
j	Slot angular separation	45°
g	Isolation gap	0.296
r_v	Via radius	0.3
t	Copper thickness	0.017

the feeds A, B, C, and D are found to be less than −14 dB across the bands.

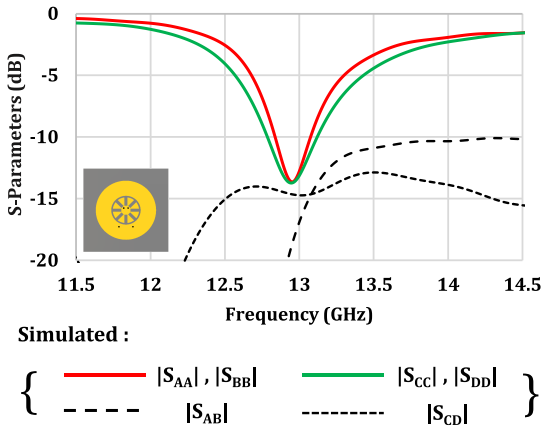

FIGURE 2. Simulated reflection coefficient ($|S_{XX}|$) and mutual coupling ($|S_{XY}|$) for the TM11 and TM21 modes of the SBMPA.

Figure 3(a) shows the 3-D radiation patterns when only the TM_{11} mode is excited, only the TM_{21} mode is excited, and when TM_{11} and TM_{21} are combined with equal amplitude (i.e., $\alpha_r = 1$) and zero phase difference (i.e., $\beta_r = 0$). This combination generates a tilted RHCP beam with a gain of 6.8 dBic, pointing toward $\theta = 35°$ from zenith in the plane $\phi = 175°$, as shown in Figures 3(b) and 3(c). For circular polarization, ports A and B as well as C and D are maintained in quadrature phase [18]. By adjusting these phases (quadrature lead, lag, or equal phase), polarization reconfigurability can be achieved.

Although the SBMPA structure is physically symmetric, the combined radiation pattern is tilted due to the deliberate superposition of the TM_{11} axial mode and TM_{21} conical mode with controlled relative amplitudes and phases. This constructive interference directs the beam toward $\theta \approx 35°$ without requiring any geometric asymmetry. Such tilting through mode combination is a standard technique in multimode patch antennas.

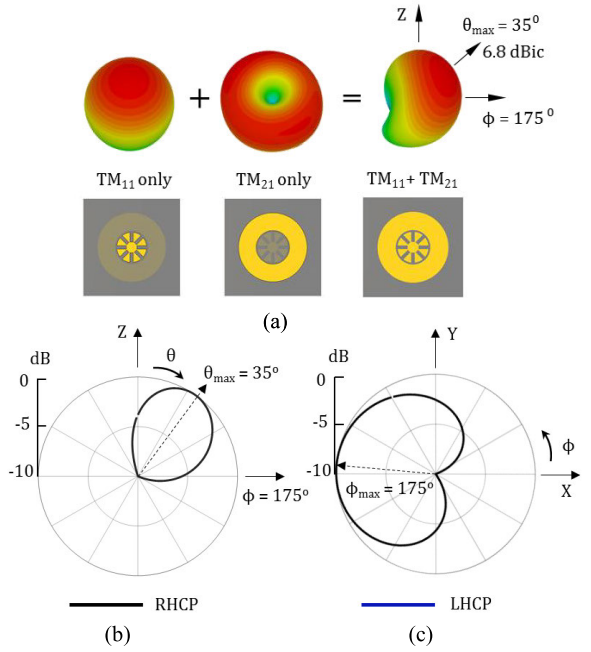

FIGURE 3. (a) 3-D patterns for the TM11 and TM21 radiating modes of SBMPA and for its combined radiations. Normalized polar plots of the tilted beam in (b) elevation plane of $\phi = 175°$ and (c) the azimuth plane of $\theta = 35°$.

The axial ratios of the inner patch and annular ring across the operational bandwidth are shown in Figure 4. The inner patch axial ratio remains below 3 dB across the operational bandwidth, while the annular ring axial ratio remains below 3.5 dB at $\phi = 40°$ and $\theta = 40°$. These results demonstrate the element's capability to support circular polarization, which can be reconfigured between RHCP, LHCP, and linear (if desired) polarization by electronically controlling the relative phase of the quadrature feeds.

Simulated axial ratios in Figure 4 are for the inner patch at $\theta = 0°$ and for the annular ring at $\theta = 40°$, showing the potential for circular polarization reconfiguration (RHCP and LHCP) through electronic phase control of the quadrature feeds. Although the SBMPA architecture is theoretically capable of generating linear polarization (LP) by applying a 0° phase difference to the quadrature feeds, the current study focuses exclusively on circular polarization (CP) for satellite applications. In other words, while LP operation is a functional feature of the design, no study to this effect is presented in this paper.

With a quadrature-feeding mechanism, the SBMPA enables a circular polarization reconfigurable radiation pattern [19], [20], [21]. When feed A and B have equal amplitude and a 90° phase difference, the slotted circular patch generates a Right-Hand Circularly Polarized (RHCP) axial beam with a gain of 6.9 dBic. If the same conditions apply to feed D and C, the annular patch generates a RHCP conical beam in the azimuth plane at $\theta_{max} = 50°$ with a gain of 3.9 dBic. Figure 5 displays the surface currents over half the period of excitation at 12.9 GHz for the two

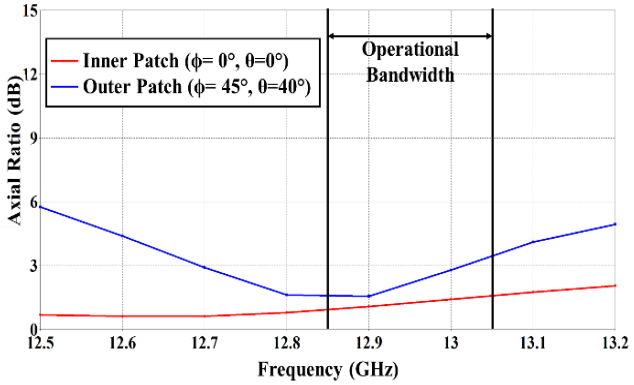

FIGURE 4. Simulated axial ratio of the inner antenna patch at $\theta = 0°$ and the outer antenna patch at $\theta = 40°$.

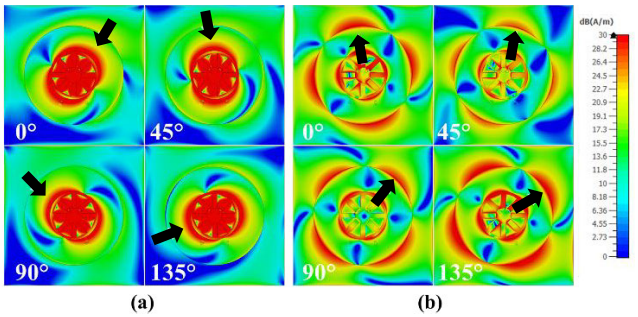

FIGURE 5. Surface currents of the antenna at 12.9 GHz when feeding (a) the inner patch and (b) the annular ring. Arrows highlight area of high magnetic field strength.

antenna components, illustrating the rotation of areas with high magnetic field strength over the time. By combining these two modes, the SBMPA generates a tilted beam. The TM_{11} and TM_{21} modes can be combined with a relative amplitude of $\alpha r = \{FD, FC\}/\{FA, FB\}$ and a relative phase difference
of $\beta r = \angle PD - \angle PA = \angle PC - \angle PB$.

By keeping the relative amplitude $\alpha r = 1$, the tilted CP radiation beam emanating from SBMPA (Figure 3) can be continuously steered in the whole of the azimuth plane (i.e.: from $\phi = 0°$ to $\phi = 360°$) by varying the phase difference βr from 0° to 360° as shown in Figure 6. As appears in Sec. III, the case $\beta r = 0°$ (corresponding to radiation beam approximately along $\phi = 0°$) is used in this work.

III. LINEAR PHASED ARRAY OF FOUR SBMPAs

To increase the gain and provide scanning in elevation, four of the SBMPA specified in Sec. II are arranged in a 1-D array as shown in Figure 7. The feed layouts are so arranged to enable a RHCP radiation pattern. To implement the feeds, two dielectric layers with a ground plane between them are used. The antenna conductors are etched on the top dielectric layer and the feedlines on the bottom layer, as shown in Figure 7. Details of the feed lines and the vias/pins connecting the feeds to the antenna are shown in Figure 8.

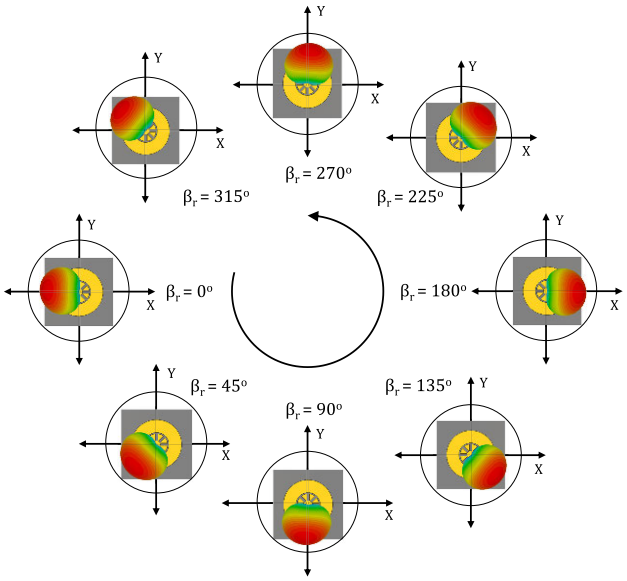

FIGURE 6. Beam rotation capability of SBMPA in azimuth plane with variation of βr from 0° to 360° (where $\alpha r = 1$).

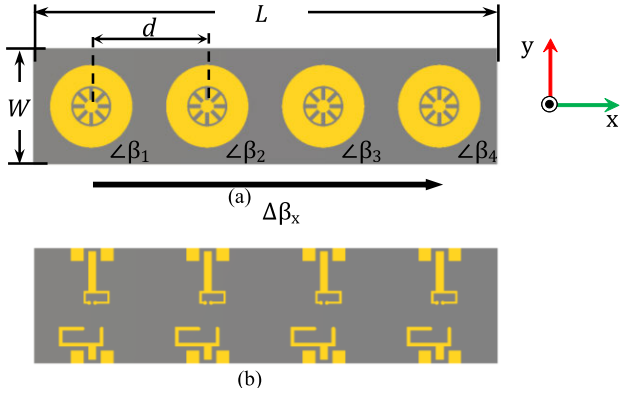

FIGURE 7. (a) Top view: 1 × 4 array geometry of the SBMPA, and (b) Bottom view: the feedlines.

Figure 8 (a) shows the side-view of the antenna layers including the feeding vias with a radius of 0.3 mm. The two substrate layers integrated are Rogers RO4350B material with a plated copper thickness of 17μm [23]. The total thickness of the two substrates including the in-between copper sheet (acting as ground plane) is H = 1.53 mm where substrate thicknesses are $H_1 = 1.02$ mm and $H_2 = 0.51$ mm. In Figure 8 (b) depicting the bottom view, the feeding mechanism for each SBMPA is shown. The feedlines are designed to provide 90° phase delay in ports of the quadrature pair to generate a RHCP axial beam and a RHCP conical beam for the inner patch and the annular ring, respectively. To match to the 50 Ω input impedance, the feedlines for the inner patch is optimized leading to dimensions $L_1 = 6.05$ mm, $L_2 = 2.02$ mm, $L_3 = 1.84$ mm, $L_4 = 0.75$ mm, $W_1 = 1.1$ mm and $W_2 = 0.32$ mm while the optimized dimensions of the feedlines to excite the outer ring are $L_5 = 2.4$ mm, $L_6 = 3.42$ mm, $L_7 = 2.76$ mm, $L_8 = 2.1$ mm and $W_3 = 0.53$ mm.

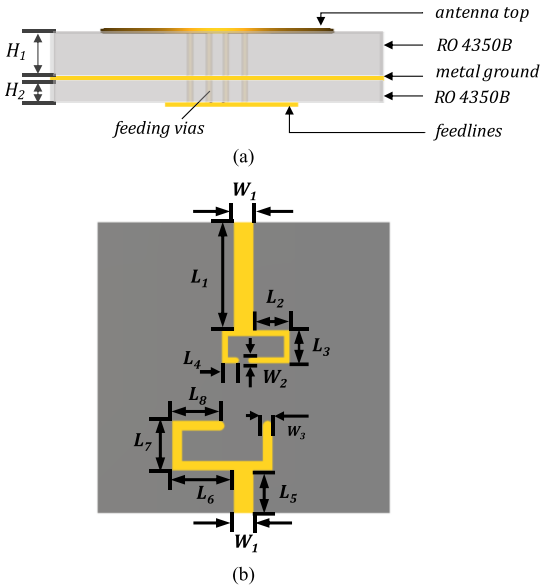

FIGURE 8. (a) Side-view of the SBMPA with stacked feedline structure. (b) Bottom view of the SBMPA showing one of the feedline layouts.

These feedline dimensions are calculated so as to maintain an impedance of 50 Ω from the connector to the antenna. Their approximate values can be found using equation (1) [24]. The approximate calculation does not take into account the metal thickness, so optimization is required after the approximate calculation to obtain the final values.

$$Z_0 = \frac{120\pi}{\sqrt{\varepsilon_{eff}} \times [\frac{W}{H} + 1.393 + \frac{2}{3} ln(\frac{W}{H} + 1.444)]} \quad (1)$$

The length of the feedlines is determined from the electrical wavelength (λ_g) at the target frequency (f) of 12.85 GHz such that there is a difference of $\lambda_g/4$ between the first and second feedline. The electrical wavelength is calculated by equation [25]:

$$\lambda_g = \frac{c_0}{f\sqrt{\varepsilon_{\text{eff}}}} \quad (2)$$

Figure 9 shows the fabricated prototype of the linear array shown in Figure 7. The conductor patterns of the antennas and the feed lines (circuits) including 50 Ω connectors (P_1 to P_8) are observable in the photographs. Also, clear in the pictures is the two dielectric layers shown in the schematic in Figure 8 (a), which are bolted together in the antenna assembly. The overall size of the array is W × L × H = 16 mm × 64 mm (= 4 × 16 mm) × 1.53 mm. The distance between two adjacent radiating elements is d = 16 mm (≈ 0.68 λ at the operating frequency 12.85 GHz). With two feeding ports per element, the SBMPA array has 8 excitation terminals in total. The connectors used at each port are SMP type and are edge mounted to the PCBs.

In the fabricated prototype, the two RO4350B substrate layers are mechanically aligned and fastened using non-conductive nylon screws positioned symmetrically around the array periphery and near the center to ensure secured assembly without interfering with the radiating or feeding regions. The screws serve purely as mechanical fasteners and have no electrical function, while electrical interconnection between the layers is achieved exclusively through plated through-holes (vias), ensuring reliable RF continuity between the feedlines and antenna patches. During assembly, the screws were hand-tightened uniformly to provide consistent mechanical pressure while avoiding substrate bending or air-gap formation. Particular care was taken to minimize air gaps between the dielectric/substrate layers while ensuring solid via connections. The resulting alignment tolerance was within ±0.1 mm, consistent with standard PCB fabrication accuracy, and was verified visually and mechanically during assembly. This alignment tolerance was found to have negligible impact on the measured impedance and radiation performance.

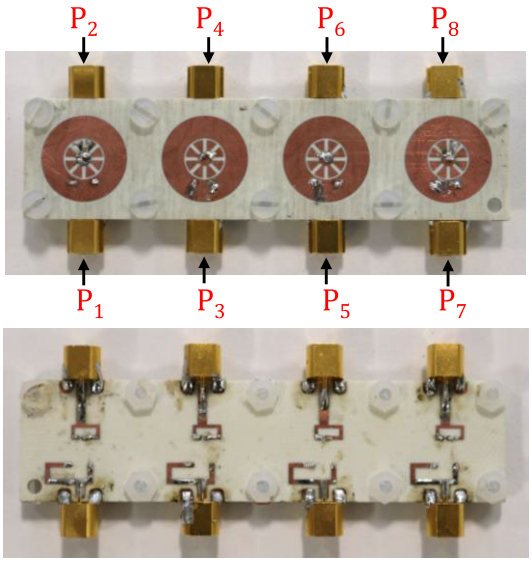

FIGURE 9. Top (radiating elements) and bottom (feed circuits) view of the fabricated prototype array of the 1 × 4 SBMPA.

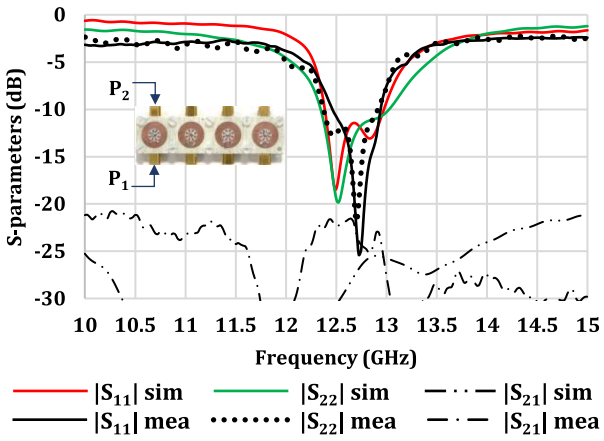

FIGURE 10. Reflection coefficients and isolations of the two radiating sections (slotted circular patch and annular ring) for the first radiating element in the 1 × 4 SBMPA array fabricated/prototype.

Figure 10 displays the simulated reflection coefficient of the antenna and feed design, indicating $|S_{11}| < -10$ dB

from 12.4 GHz to 13 GHz for both the nested patch and the annular ring for the first element in the array. In the same figure, the measured results for the same two ports of the first element in the fabricated 1 × 4 array prototype are presented, which demonstrate an impedance bandwidth from 12.5 GHz to 12.9 GHz. It should be noted that the relatively narrow impedance bandwidth (∼1.5%) corresponds to the single SBMPA element. In the full array operation, the effective bandwidth increases due to mutual coupling and the feed network, reaching approximately 4.72% in simulation and 3.1% in measurement. This bandwidth (about 350 MHz) is sufficient for many practical Ku-band satellite communication applications.

A slight upward shift in the measured resonance frequency compared to simulation (approximately 0.3 GHz) is observed in Figure 10. This discrepancy is mainly due to fabrication tolerances at Ku-band frequencies, including small variations in slot dimensions, annular ring radius, and substrate thickness, as well as, due to the presence of air gaps between stacked dielectric layers. Additional contributions arise from soldering and transition effects associated with the SMP connectors and vertical feeding vias, which are not fully captured in the idealized simulation model. Such frequency shifts are common in compact Ku-band phased-array implementations and remain within acceptable practical limits.

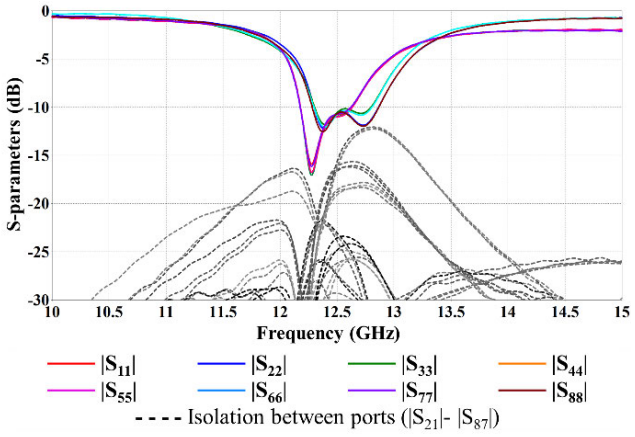

FIGURE 11. Simulation results of reflection coefficients and isolations for all ports of the 1 × 4 SBMPA array prototype.

Figure 11 presents the simulated reflection coefficient and isolation results for all ports in the 1 × 4 SBMPA array. Due to mutual coupling between the elements, the resonance frequencies of the inner patch and outer annular ring are slightly shifted to lower frequencies, with the inner patch working over 12.18–12.64 GHz and the annular ring over 12.30–12.81 GHz, where $|S_{11}|$ remains below −10 dB. The relatively higher mutual coupling (typically < −14 dB) occurs primarily between adjacent inner patch ports (e.g., P_2–P_3) and outer annular ring ports (e.g., P_6–P_7), which are closest within the array. The coupling arises from predictable near-field interactions and remains within acceptable limits for practical array operation. The fabricated prototype exhibits a slight upward operating frequency (band) shift due to minor fabrication tolerances, including air gaps between stacked substrate layers and soldering variations at SMP connectors, feed lines, and vertical feeding vias. Despite these effects, the measured array gain and beam steering performance remain stable, with a maximum variation of ±1 dB across the scanned range, indicating that the impact of mutual coupling on practical array operation has been negligible.

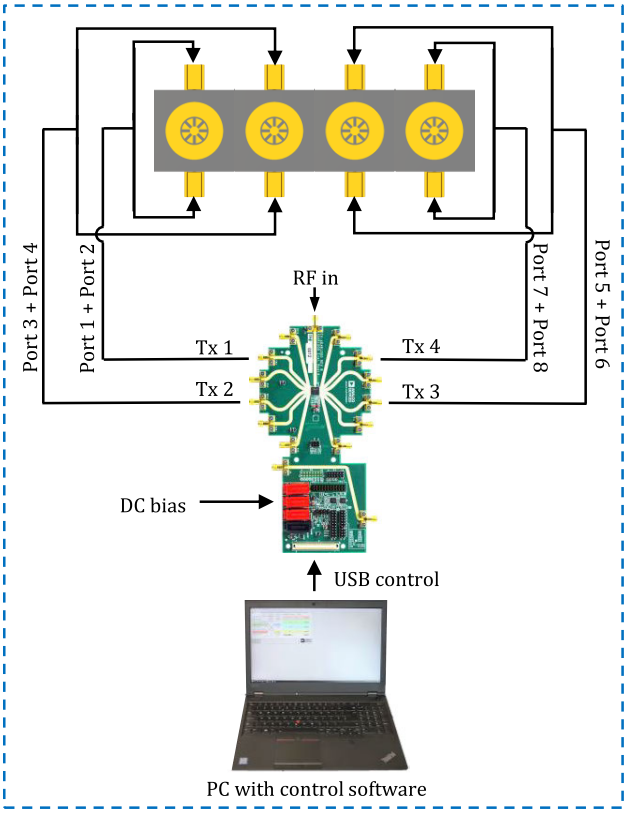

FIGURE 12. Experimental setup for the measurement of the beam scanning capability of the linear SBMPA array in a SATiMO chamber.

To assess the array radiation performance, it is placed within the experimental setup shown in Figure 12. Four 3-dB power dividers are used to feed the complete SBMPA array. Each SBMPA receives equal power and 0° phase difference (between its two radiating sections). As shown earlier, under this condition the SBMPA beam is directed along $\phi = 180°$ (as shown in Figure 6 for $\beta r = 0$). To steer the array beam in the elevation plane, a digital beam-former known as Analog Devices ADAR 1000 is employed to feed the power dividers and apply phase shifts.

The ADAR 1000 having 6-bit phase resolution (360° range) and up to 31 dB of gain adjustment is a four-channel Ku-band beamformer IC capable of providing independent phase and gain control for each channel. In the measurement setup, the four RF output ports of the ADAR1000 were connected to the input ports of the four SBMPA array elements through coaxial SMP connectors, allowing precise control of

TABLE 2. Excitation phase values for elevation plane scanning.

θ_{max}	-2^o	-18^o	-30^o	-47^o
$\angle\beta_1$	0º	0º	0º	0º
$\angle\beta_2$	0º	60º	120º	180º
$\angle\beta_3$	0º	120º	240º	360º
$\angle\beta_4$	0º	180º	360º	540º

the excitation phase ($\angle\beta_x$) as defined in Table 2. The device was programmed via a serial peripheral interface (SPI) using a computer-controlled board to set the required phase states for each scanning angle.

The radiation patterns and gains were measured in a SATiMO near-field anechoic chamber, which automatically transforms near-field data into far-field results. The antenna under test was fed through calibrated coaxial cables from the ADAR1000 outputs. The absolute gain in dBic was determined using the standard gain-substitution method: first, a reference circularly polarized horn antenna with known gain was measured under identical conditions; then, the SBMPA array was measured, and the difference in received power yielded the array gain in dBic. The RHCP and LHCP components were recorded using dual-polarized probes within the chamber, enabling evaluation of polarization purity and axial ratio.

Figure 13 shows the beam scanning performance of the array, operating in RHCP, at 12.85 GHz in the elevation plane $\phi = 0°$, considering that the progressive phase shift over the SBMPAs in the array is defined as $\angle\beta1 = 0°$, $\angle\beta2 = \angle\beta x$, $\angle\beta3 = \angle2\beta x$, and $\angle\beta4 = \angle3\beta x$. If the phase shift is set to $\angle\beta x = 0°$, the array raises a beam of a gain of 9.1 dBic in the broadside direction of $(\theta, \phi) = (-2°, 0^0)$.

In simulation, when all array elements are excited in phase ($\beta_x = 0°$), the main beam is directed at $\theta = -2°$ rather than the exact broadside (0°). This slight offset arises from small asymmetries in the simulated feed network and element arrangement, combined with mutual coupling effects between adjacent SBMPAs. Such minor deviations are typical in compact phased arrays and remain within the acceptable margin for design accuracy.

The simulated and two examples of measured radiation patterns (using a calibrated SATiMO anechoic chamber) shown in Figures 13 and 14 demonstrate strong consistency for beam steering angles of –18° and –47°. The striking agreement observed in both cases results from correct full-wave electromagnetic modelling, including realistic material and connector specifications, and from good fabrication of the prototype. The patterns are normalized to the maximum gain, which makes minor amplitude differences less visually distinguishable. Small discrepancies (within 0.5–1 dB) are present in the measured sidelobes and are within expected experimental uncertainty, confirming the validity of the simulation results.

To ensure transparency regarding the experimental scope, it is noted that the positive-angle steering results

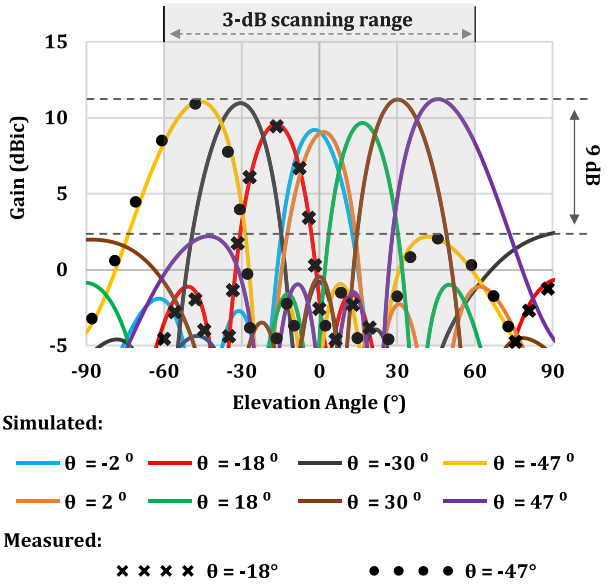

FIGURE 13. Beam scanning performance of the 1 × 4 SBMPA array at the test frequency 12.85 GHz in elevation plane $\phi = 0°$. The labeled arrows indicate the maximum grating lobe levels is approximately 9 dB below the main beam peaks.

(+18°, +30°, and +47°) are provided via simulation to demonstrate symmetric performance, while experimental validation focused on the negative-angle steering range.

With a phase shift of $\angle\beta_x = 180°$, the array beam steers to $(\theta, \phi) = (-47°, 0°)$ with a maximum gain of 11.2 dBic. The −3 dB beam edge extends to approximately $(\theta, \phi) = (-60°, 0°)$. Therefore, the array achieves beam steering up to −47° with −3 dB coverage extending to −60°. As shown in Figure 13, the gain variation across the ±60° scan range remains within approximately 2 dB (10.2 ± 1 dB). The phase shifts for other beam positions are listed in Table 2.

The highest grating lobes appear at approximately −9 dB below the main lobe peak, as annotated in Figure 13. These lobes occur symmetrically on either side of the main beam, consistent with the element spacing of d = 0.68λ, and their impact on array performance is minimal as the main lobe gain remains stable across all scanned angles.

For the extreme $\angle\beta_x = 180°$ case, the grating lobes are at least 9 dB below the main lobe maximum. To scan in the opposite direction, the relative phase between the TM_{11} and TM_{21} modes is set to $\beta_r = 180°$ (Figure 4), producing the correct RHCP unit pattern. The phase values in Table 2 are cumulative across the four array elements; for example, $\angle\beta_4 = 540°$ corresponds to 180° plus 360° but indicating the total progressive phase shift from the first to the fourth element.

In Figure 14, the simulated and measured RHCP and LHCP radiation patterns of the array are shown when the beam is steered in the direction of $(\theta, \phi) = (-18°, 180^0)$ and $(\theta, \phi) = (-47°, 180^0)$ corresponding to progressive phase $\angle\beta x = 60°$ and $\angle\beta x = 180°$ respectively (Table 2), which are in good agreement. It can be observed that the

TABLE 3. Performance comparison between the proposed configuration and reported counterparts.

Work	No. of Elements	Frequency/ Band	Peak Gain	Beam Scanning Range	Polarization
Valavan et al. 2014 [9]	9×9 (81)	X-band (dual-band, ratio 1.4:1)	—	±60° (low band), ±50° (high band)	LP
Ding et al. 2013 [11]	1×4 (4 elements)	mmWave	~12 dBi	±75°	LP
Sun et al. 2020 [12]	8×8	X/Ku-band	~17 dBi	±60° (both planes)	LP
Li et al. 2013 [13]	4×4	X-band	~7–8 dBi	±30°	LP (reconfigurable element factor)
Pal et al. 2017 [14]	2×2 (4 elements)	Ku-band (~12 GHz)	14–11.2 dBi (off-boresight); 6.5 dBi (boresight)	−60° to +60°	LP
Zhou et al. 2018 [15]	2×2 (4 elements, curl)	Ku-band (~5–6 GHz in paper)	12.4 dBic (mid scan); 10.5 dBic (near horizon)	~±80° (tilted CP beams)	CP (not reconfigurable)
Trinh-Van et al. 2024 [16]	Single element	Ku-band (13.4–14.5 GHz)	~7.5 dBic	Fixed	Dual-band dual-CP
Labadie et al. 2014 [17]	Single patch	L-band (1.575GHz)	~6–7 dBic	Limited (null steering)	CP (multimode)
Wang et al. 2024 [18]	4×4 (array)	Ku-band (12.5–13 GHz)	~10.5 dBic	±45° (elevation)	Dual-CP (fixed)
Babakhani & Sharma 2017 [19]	Single patch	X-band	~5-6 dBi	Limited	Triple-mode, mainly LP
Pal et al. 2020 [20]	Single SBMPA	1.575 GHz	~6–7 dBic	Tilted only (not array)	CP (tilted)
This Work (SBMPA Array)	1×4 (4 elements)	Ku-band (12.85–13.05 GHz)	9.2–11.2 dBic	±60° continuous	CP, polarization reconfigurable

magnitude difference between the RHCP and LHCP component is more than 15 dB at the scanned position $(\theta, \phi) = (-18°, 180^0)$ in the main beam direction, while at $(\theta, \phi) = (-47°, 180^0)$ it reduces to slightly smaller than 10 dB.

The ADAR1000 phase shifter was used to provide programmable phase control for each array element. Cumulative phase shifts for beam steering are listed in Table 2. Uniform amplitude excitation was applied to all elements.

The main beam direction in the elevation plane is dictated by the progressive phase shift (β_x) across the array elements. Conversely, switching between RHCP and LHCP is achieved by reversing the quadrature phase relationship at the feeding ports of each SBMPA element (i.e., transitioning between $+90°$ and $-90°$). Because the progressive phase distribution remains constant during polarization switching, the main beam direction is preserved across both states, ensuring that only the sense of circular polarization is altered. The array was calibrated using a vector network analyzer to verify the phase response of each channel, and any phase offsets were corrected in the ADAR1000 programming. This ensures correct phase progression and desired RHCP/LHCP polarization for beam steering.

IV. PERFORMANCE COMPARSION

The performance of the proposed 1 × 4 SBMPA array is contrasted against previously reported designs in terms of the number of elements, operating frequency band, gain, beam scanning capability, and polarization characteristics, as summarized in Table 3. The array achieves a peak gain of 9.2–11.2 dBic, comparable to other planar arrays such as those in [11] (~12 dBi) and [12] (~17 dBi), while maintaining a significantly more compact structure. A key advantage of the proposed design is its low gain variation of ±1 dB across a wide scanning range of ±60°, outperforming earlier designs such as those in [14], which exhibits a gain reduction from 14 dBi to 6.5 dBi, and [15] which demonstrates a variation of approximately 4 dB.

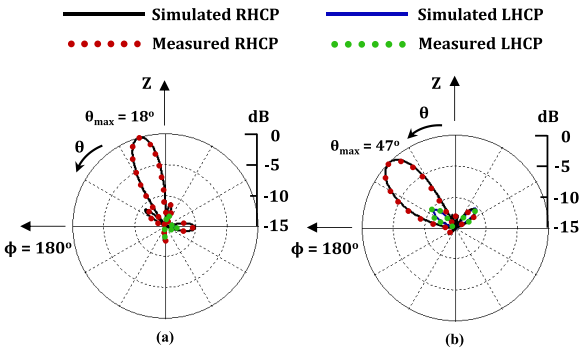

FIGURE 14. Simulated and measured RHCP and LHCP radiation patterns of the 1 × 4 SBMPA array at 12.85 GHz, for beam position at (a) $\theta = -18°$ and (b) $\theta = -47°$ in the elevation plane of $\phi = 180°$.

Recently reported Ku-band antennas, such as those in [16] and [18], have also achieved promising circularly polarized performance within compact form factors. However, both exhibit limited or fixed beam steering capability. The four-port dual-band dual-polarized antenna presented in [16] achieves approximately 7.5 dBic gain but operates with a fixed beam. Specifically, while the 4×4 array in [18] utilizes sixteen elements to achieve ∼10.5 dBic gain with a scanning range to ±45°, the proposed 1×4 SBMPA array achieves comparable gain (up to 11.2 dBic) with only four elements. Furthermore, the SBMPA design offers superior scanning coverage of ±60° and incorporates full polarization agility, whereas the architecture in [18] is restricted to fixed dual-CP operation without reconfigurability.

Furthermore, the moderate-complexity stacked feedline architecture adopted in this work simplifies fabrication compared to the more intricate feeding networks reported in [9], [10], [11], [12]. The presented array ability to support circular polarization with reconfigurability enhances its adaptability to diverse communication scenarios, whereas many existing designs remain limited to linear or fixed circular polarization modes [15], [16], [17], [18].

Overall, the comparative analysis presented in Table 3 (considering previous works [9], [10], [11], [12], [13], [14], [15], [16], [17], [18]) clearly indicates that the proposed SBMPA array demonstrates a compact, efficient, and polarization-reconfigurable solution for Ku-band applications requiring wide-angle beam steering and stable radiation characteristics,

V. CONCLUSION

This work presented a Ku-band pattern-reconfigurable slot-based microstrip patch antenna and a four-element circularly polarized linear phased array constructed using these unit elements. The antenna operates over the 12.85–13.05 GHz band and can produce an azimuth steerable circularly polarized tilted beam with a gain of 6.8 dBic. When incorporated into the linear array, an elevation beam steering up to −47° was experimentally achieved, with −3 dB coverage extending to −60°, while the array gain varied minimally from 9.2 dBic in the broadside direction to 11.2 dBic at the peak and 10.2 dBic at the scan edges, corresponding to a maximum ±1 dB variation. The fully fabricated array prototype, benefitting from a specially designed feedline, demonstrated measurements that closely matched theoretical predictions. It should be noted that while the array capability in wide-angle scanning is validated experimentally for negative angles, the symmetric performance for positive elevation angles is substantiated through simulation. With its combination of high gain, wide-angle beam steering, and circular polarization, the proposed array is highly suitable for on-the-move satellite communication, including applications in land vehicles, UAVs, IoT devices, and small vessels. Further research will address the thermal stability and efficiency of the array considering variations in substrate and copper patterns with temperature and material specifications, and will also examine the mechanical robustness of the feeding network to ensure reliable operation across the diverse environmental conditions typical of industrial applications of the array.

ACKNOWLEGMENT

The authors would also like to thank Dr. Benjamin Falkner and Dr. Hengyi Zhou for their contributions to this project.

REFERENCES

[1] A. G. Derneryd, "Microstrip array antenna," in *Proc. 6th Eur. Microw. Conf.*, Rome, Italy, Oct. 1976, pp. 339–343.
[2] R. J. Mailloux, J. McIlvenna, and N. Kernweis, "Microstrip array technology," *IEEE Trans. Antennas Propagat*, vol. AP-29, no. 1, pp. 25–37, Jan. 1981.
[3] G. C. Huang, M. F. Iskander, M. Hoque, S. R. Goodall, and T. Bocskor, "Antenna array design and system for directional networking," *IEEE Antennas Wireless Propag. Lett.*, vol. 14, pp. 1141–1144, 2015.
[4] F. Qin, S. S. Gao, Q. Luo, C.-X. Mao, C. Gu, G. Wei, J. Xu, J. Li, C. Wu, K. Zheng, and S. Zheng, "A simple low-cost shared-aperture dual-band dual-polarized high-gain antenna for synthetic aperture radars," *IEEE Trans. Antennas Propag.*, vol. 64, no. 7, pp. 2914–2922, Jul. 2016.
[5] G. Han, B. Du, W. Wu, and B. Yang, "A novel hybrid phased array antenna for satellite communication on-the-move in Ku-band," *IEEE Trans. Antennas Propag.*, vol. 63, no. 4, pp. 1375–1383, Apr. 2015.
[6] T. Lambard, O. Lafond, M. Himdi, H. Jeuland, S. Bolioli, and L. Le Coq, "Ka-band phased array antenna for high-data-rate SATCOM," *IEEE Antennas Wireless Propag. Lett.*, vol. 11, pp. 256–259, 2012.
[7] R. J. Mailloux, *Phased Array Antenna Handbook* (Artech House Antennas and Propagation Library), 2nd ed., Norwood, MA, USA: Artech, 2008.
[8] C. A. Balanis, *Antenna Theory, Analysis and Design*, 2nd ed., Hoboken, NJ, USA: Wiley, 1997.
[9] S. E. Valavan, D. Tran, A. G. Yarovoy, and A. G. Roederer, "Planar dual-band wide-scan phased array in X-band," *IEEE Trans. Antennas Propag.*, vol. 62, no. 10, pp. 5370–5375, Oct. 2014.
[10] R. Wang, B.-Z. Wang, X. Ding, and X.-S. Yang, "Planar phased array with wide-angle scanning performance based on image theory," *IEEE Trans. Antennas Propag.*, vol. 63, no. 9, pp. 3908–3917, Sep. 2015.
[11] X. Ding, B.-Z. Wang, and G.-Q. He, "Research on a millimeter-wave phased array with wide-angle scanning performance," *IEEE Trans. Antennas Propag.*, vol. 61, no. 10, pp. 5319–5324, Oct. 2013.
[12] B.-F. Sun, X. Ding, Y.-F. Cheng, and W. Shao, "2-D wide-angle scanning phased array with hybrid patch mode technique," *IEEE Antennas Wireless Propag. Lett.*, vol. 19, no. 4, pp. 700–704, Apr. 2020.
[13] Z. Li, D. Rodrigo, L. Jofre, and B. A. Cetiner, "A new class of antenna array with a reconfigurable element factor," *IEEE Trans. Antennas Propag.*, vol. 61, no. 4, pp. 1947–1955, Apr. 2013.
[14] A. Pal, A. Mehta, D. Mirshekar-Syahkal, and H. Nakano, "2×2 phased array consisting of square loop antennas for high gain wide angle scanning with low grating lobes," *IEEE Trans. Antennas Propag.*, vol. 65, no. 2, pp. 576–583, Feb. 2017.

[15] H. Zhou, A. Pal, A. Mehta, H. Nakano, A. Modigliana, T. Arampatzis, and P. Howland, "Reconfigurable phased array antenna consisting of high-gain high-tilt circularly polarized four-arm curl elements for near horizon scanning satellite applications," *IEEE Antennas Wireless Propag. Lett.*, vol. 17, no. 12, pp. 2324–2328, Dec. 2018.
[16] S. Trinh-Van, W. Y. Yang, H. W. Cho, and K. C. Hwang, "A four-port dual-band dual-polarized antenna for Ku-band satellite communications," *Appl. Sci.*, vol. 14, no. 7, p. 2730, Mar. 2024, doi: 10.3390/app14072730.
[17] Y. S. Gurbet and S. Doğu, "Comprehensive review of Ku, K, and Ka band antenna designs: Applications in CubeSats," *Int. J. Aeronaut. Space Sci.*, vol. 27, no. 1, pp. 447–496, Jan. 2026, doi: 10.1007/s42405-025-00989-5.
[18] W. Wang, X. Li, and J. Zhou, "A low-profile dual-circularly polarized Ku-band microstrip antenna array for satellite communications," *IEEE Antennas Wireless Propag. Lett.*, vol. 23, no. 5, pp. 875–879, May 2024.
[19] N. R. Labadie, S. K. Sharma, and G. M. Rebeiz, "A circularly polarized multiple radiating mode microstrip antenna for satellite receive applications," *IEEE Trans. Antennas Propag.*, vol. 62, no. 7, pp. 3490–3500, Jul. 2014.
[20] B. Babakhani and S. K. Sharma, "Dual null steering and limited beam peak steering using triple-mode circular microstrip patch antenna," *IEEE Trans. Antennas Propag.*, vol. 65, no. 8, pp. 3838–3848, Aug. 2017.
[21] A. Pal, A. Mehta, A. Skippins, P. Spicer, and D. Mirshekar-Syahkal, "Novel interference suppression null steering antenna system for high precision positioning," *IEEE Access*, vol. 8, pp. 77779–77787, 2020.
[22] *CST Studio Suit*. Dassault Systèmes SE, Vélizy-Villacoublay, France. Accessed: Dec. 3, 2022. [Online]. Available: www.3ds.com/products-services/simulia/products/cst-studio-suite
[23] *RO4350BTM Laminates*. Rogers Corporation. Accessed: Nov. 30, 2022. [Online]. Available: https://rogerscorp.com/advanced-connectivity-solutions/ro4000-series-laminates/ro4350b-laminates
[24] C. A. Balanis, *Antenna Theory: Analysis and Design*, 4th ed., Hoboken, NJ, USA: Wiley, 2016.
[25] D. M. Pozar, *Microwave Engineering*, 4th ed., Hoboken, NJ, USA: Wiley, 2011.

AMIT MEHTA (Senior Member, IEEE) received the B.Eng. degree in electronics and telecommunication from the University of Pune, India, and the M.Sc. degree in telecommunications and information networks and the Ph.D. degree in smart reconfigurable antennas from the University of Essex, U.K. He is currently a Professor and the Director of the Antenna Research Group, Swansea University, U.K., where his core research interests are wireless communications, microwave systems, and antennas. He is leading large project teams on 5G, adaptive antennas for GNSS, high-throughput satellite communications, the IoT, and mm waves. He has successfully supervised more than 20 postgraduate research theses. He has more than 100 technical publications. He holds three patents on the invention of the steerable beam smart antennas and concealed weapons detection systems.

RAWAD W. ASFOUR (Member, IEEE) received the B.Sc. degree (Hons.) in electrical and electronic engineering from Benghazi University, Benghazi, Libya, the M.Sc. degree in mobile and satellite communications from the University of South Wales, U.K., in 2017, and the Ph.D. degree in electrical and electronic engineering from the University of Sheffield, Sheffield, U.K., in 2024. He is currently a Senior Research Officer with the University of Essex, Colchester, U.K. His research interests include full-duplex communication systems, phased-array antennas, dielectric resonator antennas (DRAs), reconfigurable intelligent surfaces (RIS), and millimeter-wave (mmWave) communication technologies. He was awarded the Master's Award of Excellence from the University of South Wales.

HISAMATSU NAKANO (Life Fellow, IEEE) has been with Hosei University, since 1973, where he is currently a Professor Emeritus and a special appointment Researcher with the Electromagnetic Wave Engineering Research Institute attached to the graduate school. He has held positions as a Visiting Associate Professor with Syracuse University, from March to September 1981, a Visiting Professor with the University of Manitoba, from March to September 1986, the University of California at Los Angeles, from September 1986 to March 1987, and Swansea University, U.K., from July 2016 to September 2019. He has published more than 330 articles in peer-reviewed journals and 11 books/book chapters, including *Low-Profile Natural and Metamaterial Antennas* (IEEE Press, Wiley), in 2016. His significant contributions are the development of five integral equations for line antennas in free space and printed on a dielectric substrate, the invention of an L-shaped wire/strip antenna feeding method, and the realization of numerous wideband antennas, including curl, metaspiral, metahelical, and body-of-revolution antennas. His other accomplishments include the design of antennas for GPS, personal handsets, space radio, electronic toll collection, RFID, UWB, and radar. He has been awarded 78 patents, including A Curl Antenna Element and Its Array, in Japan. His research interests include numerical methods for low- and high-frequency antennas and optical waveguides. He served as a member for the IEEE APS Administrative Committee, from 2000 to 2002, and a Region 10 Representative, from 2001 to 2010. He received the H. A. Wheeler Award, in 1994, the Chen-To Tai Distinguished Educator Award, in 2006, and the Distinguished Achievement Award from the IEEE Antennas and Propagation Society, in 2016. He was a recipient of the Prize for Science and Technology from Japan's Minister of Education, Culture, Sports, Science, and Technology, in 2010. He was selected as a recipient of the Antenna Award of the European Association on Antennas and Propagation (EurAAP), in 2020. He is also an Associate Editor for several scientific journals and magazines, such as *Electromagnetics* and *IEEE Antennas and Propagation Magazine*.

DARIUSH MIRHSEKAR-SYAHKAL (Life Fellow, IEEE) received the B.Sc. degree (Hons.) in electrical engineering from Tehran University, Tehran, Iran, and the M.Sc. degree in microwaves and modern optics and the Ph.D. degree from University College London, University of London, U.K. From 1979 to 1984, he was a Research Fellow with University College London, on analysis and design of microwave and millimeter-wave planar transmission lines and components and on nondestructive evaluation of materials by electromagnetic techniques. Since 1984, he has been on the staff of the University of Essex, Colchester, U.K., where he is currently a Professor and the Head of the RF and Microwave Research Laboratory, School of Computer Science and Electronic Engineering. He owns several patents and has numerous technical publications, including a book entitled *Spectral Domain Method for Microwave Integrated Circuits* (New York: Wiley), published in 1990. He has been a consultant to more than ten major international companies. His current research interests include adaptive antennas, super-compact RF filters, RF amplifier linearization, characterization and applications of liquid crystal materials at microwave and mm-wave frequencies, numerical modeling in electromagnetics and circuits, and mmWave full duplex communication systems. He is a fellow of IET and a Chartered Engineer.